An Arg/Ala-Rich Helix in the N-Terminal Region of *M. tuberculosis* FtsQ Anchors FtsZ to Membranes

Cristian A. Escobar[a,c], Souvik Dey[d], Sean T. Smrt[c], Timothy A. Cross[a,b,c,*], and Huan-Xiang Zhou[d,e,*]

[a]Institute of Molecular Biophysics and [b]Department of Chemistry and Biochemistry, Florida State University, Tallahassee, FL32306, USA

[c]National High Magnetic Field Laboratory, Tallahassee, FL32310, USA

[d]Department of Chemistry and [e]Department of Physics, University of Illinois at Chicago, Chicago, IL 60607, USA

*Correspondence should be addressed to H.X.Z. (e-mail: hzhou43@uic.edu) or T.A.C. (e-mail: timothyAcross@gmail.com).

Abstract

Mycobacteria tuberculosis (*Mtb*) inflicts a quarter of the worldwide population. Most drugs for treating tuberculosis target cell growth and division. With rising drug resistance, it becomes ever more urgent to better understand *Mtb* cell division. This process begins with the formation of the Z-ring via polymerization of FtsZ and anchoring of the Z-ring to the inner membrane. Here we show that the transmembrane protein FtsQ is a membrane anchor of the *Mtb* Z-ring. More specifically, FtsQ uses an Arg/Ala-rich helix in its otherwise disordered N-terminal cytoplasmic region to bind with the GTPase domain of FtsZ. Binding of FtsQ to the GTPase domain of FtsZ also has enormous implications for drug binding and Z-ring formation including its curvature.

In *Mycobacterium tuberculosis* (*Mtb*), FtsQ is an essential transmembrane protein that participates in the development of the divisome, the machinery responsible for bacterial cell division (*1-3*). The divisome comprises dozens of transmembrane and water-soluble proteins. While its composition can vary from organism to organism, at the heart is FtsZ, a water-soluble protein with a globular GTPase domain and a disordered C-tail; the GTPase domain polymerizes to form the Z-ring and initiate cell division. The Z-ring must be anchored to the inner membrane, via interactions with either transmembrane proteins or membrane-tethered water-soluble proteins. In *Mtb*, FtsQ is an early recruit in the developing divisome. While the *Escherichia coli* version typical of bacterial FtsQ proteins has only a short N-terminal cytoplasmic region (27 residues), the *Mtb* version is 99 residues long, prior to a single transmembrane helix and a 191-residue C-terminal periplasmic region that putatively forms a POTRA (or polypeptide transport associated) domain. The characterization of the periplasmic region is a subject of debate as the mechanistic attributes of POTRA domains remain to be demonstrated for the *Mtb* FtsQ protein (*4*). Here, we focus on the characterization of the *Mtb* FtsQ cytoplasmic region, or FtsQ1-99, and demonstrate its binding both to acidic membranes that mimic the *Mtb* inner membrane (*5*) and to *Mtb* FtsZ.

Membrane anchoring of the Z-ring is well studied in *E. coli* and *Bacillus subtilis*. Two proteins, FtsA and ZipA in *E. coli* and FtsA and SepF in *B. subtilis*, each act as membrane anchors (*6-8*). ZipA is a transmembrane protein (*9*), whereas FtsA and SepF are water-soluble proteins with an amphipathic helix for membrane tethering (*10, 11*). FtsZ uses its disordered C-tail to bind a structured domain in each of these three proteins for membrane anchoring (*11-13*). In *E. coli*, FtsA and ZipA provide redundancy in membrane anchoring, as Z-rings can form in the absence of either one of them but not both (*6*). Such redundancy is likewise provided by FtsA and SepF in *B. subtilis* (*8*). However, *Mtb* has SepF (*14*) but no FtsA, and may have another unidentified membrane anchor of the Z-ring for redundancy.

The N-terminal cytoplasmic region of FtsQ, comprising the first 99 residues, is expected to be disordered due to its high content of charged residues: nearly half of the residues are either positively charged (Arg and Lys, 21 total) or negatively charged (Asp and Glu, 20 total) (Fig. 1A). Even more strikingly, the positive and negative charges are separated, with a net negative charge of -14 for the first 44 residues and a net positive charge of +15 for the remaining 55 residues. Consistent with the expectation of disorder, the HSQC spectrum of FtsQ1-99 in solution is well-resolved, but with a narrow proton chemical shift range (7.9-8.6 ppm) (Fig. 1B). Glu40 is an outlier with a proton chemical shift of 9.2 ppm, due at least in part to its position following a Pro residue.

The assignments for the backbone H^N, N, C_α, and C_β chemical shifts are presented in Table S1. The C_α and C_β secondary chemical shifts clearly indicate an α-helix formed by residues 46-74, with $\Delta\delta C_\alpha - \Delta\delta C_\beta$ in the range of 2 to 4 ppm (Fig. S1A). Beyond this helical region, $\Delta\delta C_\alpha - \Delta\delta C_\beta$ decreases rapidly to 0 on both sides. Therefore FtsQ1-99 forms an α-helix in residues 46-74 but is otherwise disordered. This α-helix is quite long, with 29 residues. It is also notable for its composition, with 11 Arg residues, 10 Ala residues, and only 8 other amino acids. We will therefore refer to this helix as "Arg/Ala-rich". Additional support for this Arg/Ala-rich helix in an otherwise disordered background is provided by NMR backbone relaxation data (Fig. S1B-D), residual dipolar coupling data (Fig. S2A-C), and molecular dynamics (MD) simulations (Figs. S1 and S2D) (see Supplementary text 1). Paramagnetic relaxation enhancement data and MD simulations reveal that the Arg/Ala-rich helix interacts with the N-tail (residues 1-45) (Figs. S3A and S4), with the forgoing conformational characterization further validated by the agreement between measured and calculated small-angle X-ray scattering profiles (Figs. S3B) (see Supplementary text 2).

As shown by the helical wheel projection in Fig. 1C, a subset of the Ala residues in the Arg/Ala-rich helix lines a ridge along a single face of the helix. This helix is amphipathic and is expected to bind well with acidic membranes that mimic the inner

membrane of *Mtb* (*5*). Indeed, solution NMR of FtsQ1-99 in the presence of liposomes formed by POPG/POPE lipids at a 7:3 molar ratio results in the observation of only residues 1-36 in the N-tail (Fig. 2). Many of these resonances, especially from residues 20-30, are significantly shifted (Fig. 2B). Resonances of the remaining residues are all broadened beyond detection due to membrane binding. The missing resonances of the helical region (residues 46-74) is as expected. The absence of resonances from either side of the helical region may be due to motional coupling to the Arg/Ala-rich helix and additional membrane binding segments, including possibly an additional amphipathic helix at the C-terminus (Figs. S5). Due to the narrow hydrophobic arc spanned by the Ala ridge (Fig. 1C), the burial of the Arg/Ala-rich helix into membranes is expected to be shallow. MD simulations of membrane-bound FtsQ1-99 bear out this expectation (Figs. S6 and S7), and provide explanations for the significant chemical shift perturbations of residues 20-30 and the motional coupling between the helix and neighboring residues (Fig. S8) (see Supplementary text 3).

We further characterized the membrane-bound FtsQ1-99 by solid-state NMR using oriented and uniformly ^{15}N labeled samples. The PISEMA spectrum suggests a tilt angle of 74° ± 4° for the Arg/Ala-rich helix with respect to the bilayer normal (Figure S9A). Moreover, the detection (by cross polarization) of Arg sidechain ^{15}N anisotropic chemical shifts at 71 and 83 ppm (Figure S9B) documents the significant role of Arg residues from the Arg/Ala-rich helix in membrane binding. Consistent with the PISEMA data, the helix has a tilt angle of 79° ± 5° in the MD simulations, with the C-terminus more buried at the membrane interface than the N-terminus (Fig. S7A, B). Also consistent with the strong signals of the Arg sidechains in the solid-state NMR experiment, the Arg sidechains from the entire helix interact with lipid phosphates (Fig. S8C, D). With the N-terminus of the helix lifted, Arg49, Arg 50, and Arg52 reach downward for phosphates. Moving down the helix, Arg56 and Arg61 snorkel from the opposite sides of the helix, whereas Arg69 and Arg70 reach directly upward for phosphates.

Because FtsZ and FtsQ are among the earliest proteins recruited to the divisome, we wondered whether the *Mtb* FtsQ N-terminal cytoplasmic region, with its much longer length than the *E. coli* counterpart, could bind to the water-soluble FtsZ. Our pull-down assay shows that FtsQ1-99 indeed binds to *Mtb* FtsZ (Fig. 3). More specifically, it binds to the GTPase domain (residues 1-312), not to the disordered C-tail (residues 313-379) of FtsZ. The participation of the FtsZ GTPase domain in binding with another divisome protein is unusual, as it is the C-tail that binds with FtsA, ZipA, and SepF for the membrane anchoring of FtsZ (*11-13, 15*) and with FtsW at the late stage of cell division (*16*).

Solution NMR of FtsQ1-99 in the presence of *Mtb* FtsZ reveals the Arg/Ala-rich helix as the central region for binding to the FtsZ GTPase domain (Fig. 4). The resonances of the helical residues are all broadened beyond detection upon binding FtsZ, as are flanking residues 38-45 and 75-79. Once again, residues 20-30 in the N-tail experience particularly strong chemical shift perturbations. We confirmed that the FtsZ C-tail does not interact with FtsQ1-99 by solution NMR, as the HSQC spectrum of the former is unaffected by the presence of the latter (Fig. S10).

Due to the difficulty presented by the large size of the FtsZ GTPase domain, we used computational modeling to identify the likely docking site for the FtsQ Arg/Ala-rich helix. This helix is very long and also highly positively charged. Both of these features are accommodated well by the cleft between the two subdomains of the FtsZ GTPase domain (Fig. S11). At the base of this cleft is the core helix (named H7; residues 175-200 (*17*)), which, with 26 residues, nearly matches the Arg/Ala-rich helix in length. Moreover, the electrostatic surface of the GTPase domain is mostly negative, and the negative electrostatic potential is the most intense in the inter-subdomain cleft. As a plausible pose, we docked the Arg/Ala-rich helix into this cleft in a parallel direction with respect to the H7 helix and with an array of Arg residues, at positions 50, 61, and 69, within the interface (Fig. S12A). A number of salt bridges and hydrogen bonds are

formed between the two helices, including FtsQ Arg50 with FtsZ Asp178, FtsQ Glu51 with FtsZ Arg181, FtsQ Arg61 with FtsZ Glu185 and Asn189, and FtsQ Arg69 with FtsZ Thr199 (Fig. S12B, left panel). The Arg/Ala-rich helix also forms two additional salt bridges with the walls of the cleft, i.e., between FtsQ Arg55 and FtsZ Glu29 on one side and between FtsQ Arg75 and FtsZ Asp297 on the opposite side (Fig. S12B, right panel).

The binding of the FtsQ Arg/Ala-rich helix to the GTPase domain of FtsZ makes FtsQ a membrane anchor of the *Mtb* Z-ring. Because the Z-ring is formed by the polymerization of the GTPase domain, direct binding of the FtsQ Arg/Ala-rich helix keeps the Z-ring in close proximity to the inner membrane. SepF has also been characterized as a membrane anchor of the Z-ring in *B. subtilis*, *C. glutamicum*, and *Mtb* (*11, 14, 15, 19*). It is a water-soluble protein but tethers to the membrane by an amphipathic helix at its N-terminus and, in the *Mtb* version, also by Arg-rich stretches in the disordered linker preceding the FtsZ-binding core domain (*19*). The additional membrane interactions by the *Mtb* SepF linker brings the Z-ring into close proximity of the membrane. Therefore both membrane anchors, FtsQ and SepF, either together or independently, keep the *Mtb* Z-ring close to the membrane, so it can interact with and thus recruit other membrane proteins including FtsW (*16*) and CrgA (*18*) at the late stage of cell division. FtsQ also interacts with CrgA (*18*), possibly through their transmembrane helices; the tripartite interactions between FtsQ, CrgA, and the Z-ring help maintain the integrity of the late divisome.

In contrast to other divisome proteins that bind to FtsZ, FtsQ binds to the GTPase domain instead of the disordered C-tail of FtsZ. FtsQ binding to the GTPase domain potentially impacts drug binding to the same domain as well as other functions of this domain, and therefore has important consequences. In particular, the C-terminal half of the H7 helix in the GTPase domain lines a drug binding site (*20*). If the FtsQ Arg/Ala-rich helix indeed binds to the inter-subdomain cleft as modeled here (Fig. S12A), then

drug binding and FtsQ binding would interfere with each. This scenario would have enormous implications for drug development against tuberculosis.

Another important issue raised by the fact that FtsQ binds to the GTPase domain concerns the formation of the Z-ring. Because the Z-ring is formed by the polymerization of the GTPase domain, FtsQ binding could affect the polymerization process. It has been recognized that, upon initial GTP binding, FtsZ polymerizes in a straight manner, but after GTP hydrolysis into GDP, the FtsZ polymers become curved, thereby facilitating Z-ring formation (*21*). Interestingly, in the binding pose modeled here (Fig. S12A), the FtsQ Arg/Ala-rich helix does not interfere with the GTPase domains of the adjacent FtsZ monomers in curved polymers (Fig. S12C) but encounters clashes in straight polymers (Fig. S12D). In that case, FtsQ would not only anchor the Z-ring to the membrane but also stabilize its curvature.

References

1. K. J. Kieser, E. J. Rubin, How sisters grow apart: mycobacterial growth and division. *Nat Rev Microbiol* **12**, 550-562 (2014).
2. K. J. Wu *et al.*, Characterization of Conserved and Novel Septal Factors in Mycobacterium smegmatis. *J Bacteriol* **200**, 00649-00617 (2018).
3. P. Jain *et al.*, Delineating FtsQ-mediated regulation of cell division in Mycobacterium tuberculosis. *J Biol Chem* **293**, 12331-12349 (2018).
4. L. Sanchez-Pulido, D. Devos, S. Genevrois, M. Vicente, A. Valencia, POTRA: a conserved domain in the FtsQ family and a class of beta-barrel outer membrane proteins. *Trends Biochem Sci* **28**, 523-526 (2003).
5. M. Jackson, D. C. Crick, P. J. Brennan, Phosphatidylinositol Is an Essential Phospholipid of Mycobacteria. *J Biol Chem* **275**, 30092-30099 (2000).
6. S. Pichoff, J. Lutkenhaus, Unique and overlapping roles for ZipA and FtsA in septal ring assembly in *Escherichia coli*. *EMBO J* **21**, 685-693 (2002).

7. L. W. Hamoen, J.-C. Meile, W. De Jong, P. Noirot, J. Errington, SepF, a novel FtsZ-interacting protein required for a late step in cell division. *Mol Microbiol* **59**, 989-999 (2006).

8. S. Ishikawa, Y. Kawai, K. Hiramatsu, M. Kuwano, N. Ogasawara, A new FtsZ-interacting protein, YlmF, complements the activity of FtsA during progression of cell division in Bacillus subtilis. *Mol Microbiol* **60**, 1364-1380 (2006).

9. C. A. Hale, P. A. J. de Boer, Direct Binding of FtsZ to ZipA, an Essential Component of the Septal Ring Structure That Mediates Cell Division in E. coli. *Cell* **88**, 175-185 (1997).

10. S. Pichoff, J. Lutkenhaus, Tethering the Z ring to the membrane through a conserved membrane targeting sequence in FtsA. *Mol Microbiol* **55**, 1722-1734 (2005).

11. R. Duman *et al.*, Structural and genetic analyses reveal the protein SepF as a new membrane anchor for the Z ring. *Proc Natl Acad Sci U S A* **110**, E4601-E4610 (2013).

12. M. Loose, T. J. Mitchison, The bacterial cell division proteins FtsA and FtsZ self-organize into dynamic cytoskeletal patterns. *Nat Cell Biol* **16**, 38-46 (2014).

13. T. A. Cameron *et al.*, ZipA Uses a Two-Pronged FtsZ-Binding Mechanism Necessary for Cell Division. *mBio* **12**, e02529-02521 (2021).

14. S. Gola, T. Munder, S. Casonato, R. Manganelli, M. Vicente, The essential role of SepF in mycobacterial division. *Mol Microbiol* **97**, 560-576 (2015).

15. A. Sogues *et al.*, Essential dynamic interdependence of FtsZ and SepF for Z-ring and septum formation in Corynebacterium glutamicum. *Nat Commun* **11**, 1641 (2020).

16. P. Datta, A. Dasgupta, S. Bhakta, J. Basu, Interaction between FtsZ and FtsW of *Mycobacterium tuberculosis*. *J Biol Chem* **277**, 24983-24987 (2002).

17. A. K. Leung *et al.*, Structure of Mycobacterium tuberculosis FtsZ reveals unexpected, G protein-like conformational switches. *J Mol Biol* **342**, 953-970 (2004).
18. P. Plocinski *et al.*, Characterization of CrgA, a New Partner of the Mycobacterium tuberculosis Peptidoglycan Polymerization Complexes. *J Bacteriol* **193**, 3246-3256 (2011).
19. S. Dey, H. X. Zhou, Membrane Tethering of SepF, a Membrane Anchor for the *Mycobacterium tuberculosis* Z- ring. *J Mol Biol*, in press (2022).
20. P. Pradhan, W. Margolin, T. K. Beuria, Targeting the Achilles Heel of FtsZ: The Interdomain Cleft. *Front Microbiol* **12**, 732796 (2021).
21. Y. Li *et al.*, FtsZ protofilaments use a hinge-opening mechanism for constrictive force generation. *Science* **341**, 392-395 (2013).

Acknowledgments

This work was supported by National Institutes of Health Grants AI119187, GM122698, and GM118091. All NMR experiments were carried out at the National High Magnetic Field Laboratory supported by the NSF Cooperative Agreement No. 1644779 and the State of Florida.

Author contributions

T.A.C. and H.-X.Z. designed the research; C.A.E., S.D., and S. S. performed the research and analyzed the data; T.A.C. and H.-X.Z. wrote the manuscript.

Competing financial interests: The authors declare no competing financial interests.

Figure Captions

Figure 1. Sequence and conformational properties of FtsQ1-99. (A) The amino-acid sequence. The helical region is underlined, with Ala residues therein in green; acidic and basic residues are shown as red and blue, respectively, throughout the sequence. (B) ^{1}H-^{15}N HSQC spectrum of ^{13}C-^{15}N uniformly labeled FtsQ1-99 at 370 μM, acquired on an 800 MHz spectrometer at 25 °C in 20 mM of phosphate buffer (pH 6.5) with 25 mM of NaCl. (C) Helical wheel representation for residues 48-72. Acidic, basic, Ala, and other residues are shown in red, blue, green, and grey respectively. Arg49 and Arg50 define a 100° arc, in which Ala53, Ala57, Ala60, Ala64, and Ala71 fall.

Figure 2. Characterization of the binding of FtsQ1-99 with POPG/POPE membranes. (A) ^{1}H-^{15}N HSQC spectra of 50 μM ^{13}C-^{15}N uniformly labeled FtsQ1-99 in the absence (black) or presence (red) of POPG/POPE (7:3) liposomes (1:100 protein to lipid molar ratio). Acquired on an 800 MHz spectrometer at 25 °C in 20 mM of phosphate buffer (pH 6.5) with 25 mM of NaCl. (B) Chemical shift differences calculated as $\Delta\delta_{\mathrm{NH}} = \sqrt{(\Delta\delta_{\mathrm{H}})^2 + (1/6)(\Delta\delta_{\mathrm{N}})^2}$. Arrows indicate ambiguous assignments; shaded region indicates missing resonances.

Figure 3. Pull-down assay for FtsQ1-99 binding with FtsZ. (A) SDS-PAGE of aliquots collected from running His-tagged FtsQ1-99 (His-FtsQ1-99) and untagged full-length FtsZ or its GTPase domain (FtsZ-G) or C-tail (FtsZ-CT) individually through a nickel column. Abbreviations are: M, molecular-weight markers; FT, flow-through; E, elution. Arrowheads indicate the major population. (B) Corresponding results collected from running mixtures of His-FtsQ1-99 with FtsZ, FtsZ-G, or FtsZ-CT through a nickel column. Arrowheads indicate that FtsZ and FtsZ-G as well as His-FtsQ1-99 are found in the elution fractions but FtsZ-CT is only found in the flow-through fraction.

Figure 4. Characterization of the binding of FtsQ1-99 with FtsZ. (A) ^{1}H-^{15}N HSQC spectra of 50 μM ^{13}C-^{15}N uniformly labeled FtsQ1-99 in the absence (black) or presence (red) of 50 μM FtsZ. Acquired on an 800 MHz spectrometer at 25 °C in 20 mM of

phosphate buffer (pH 6.5) with 25 mM of NaCl. (B) Chemical shift differences calculated as $\Delta\delta_{\mathrm{NH}} = \sqrt{(\Delta\delta_{\mathrm{H}})^2 + (1/6)(\Delta\delta_{\mathrm{N}})^2}$. Arrows indicate ambiguous assignments; shaded region indicates missing resonances.

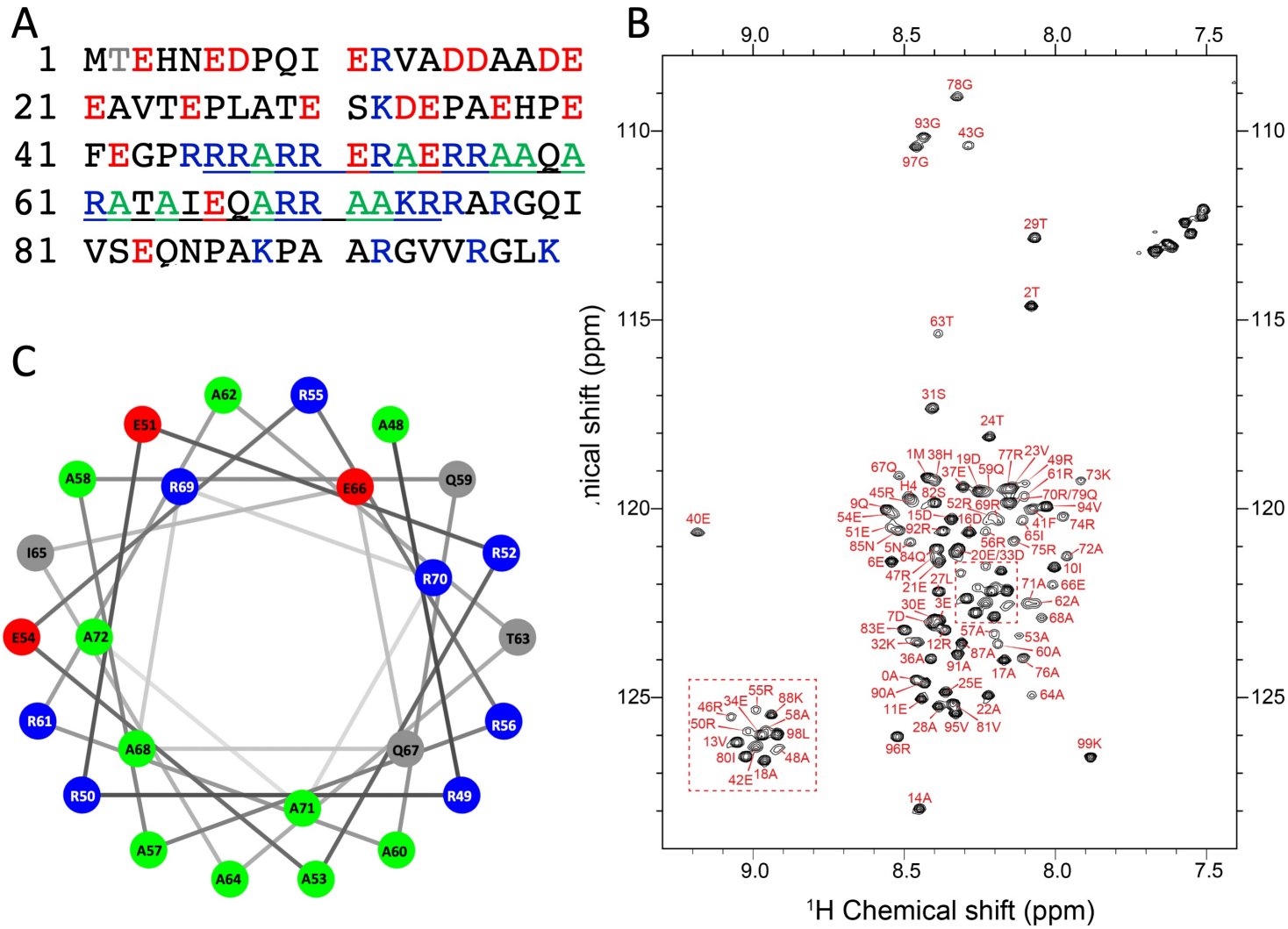
A
1 MTEHNEDPQI ERVADDAADE
21 EAVTEPLATE SKDEPAEHPE
41 FEGPRRRARR ERAERRAAQA
61 RATAIEQARR AAKRRARGQI
81 VSEQNPAKPA ARGVVRGLK
B
9.0
8.5
8.0
7.5
110
115
120
125
nical shift (ppm)
¹H Chemical shift (ppm)
C
A62
R55
E51
A48
A58
R69
E66
Q59
I65
R52
R70
E54
A72
T63
R61
R56
A68
Q67
R50
R49
A71
A57
A60
A64
A53

Figure 1

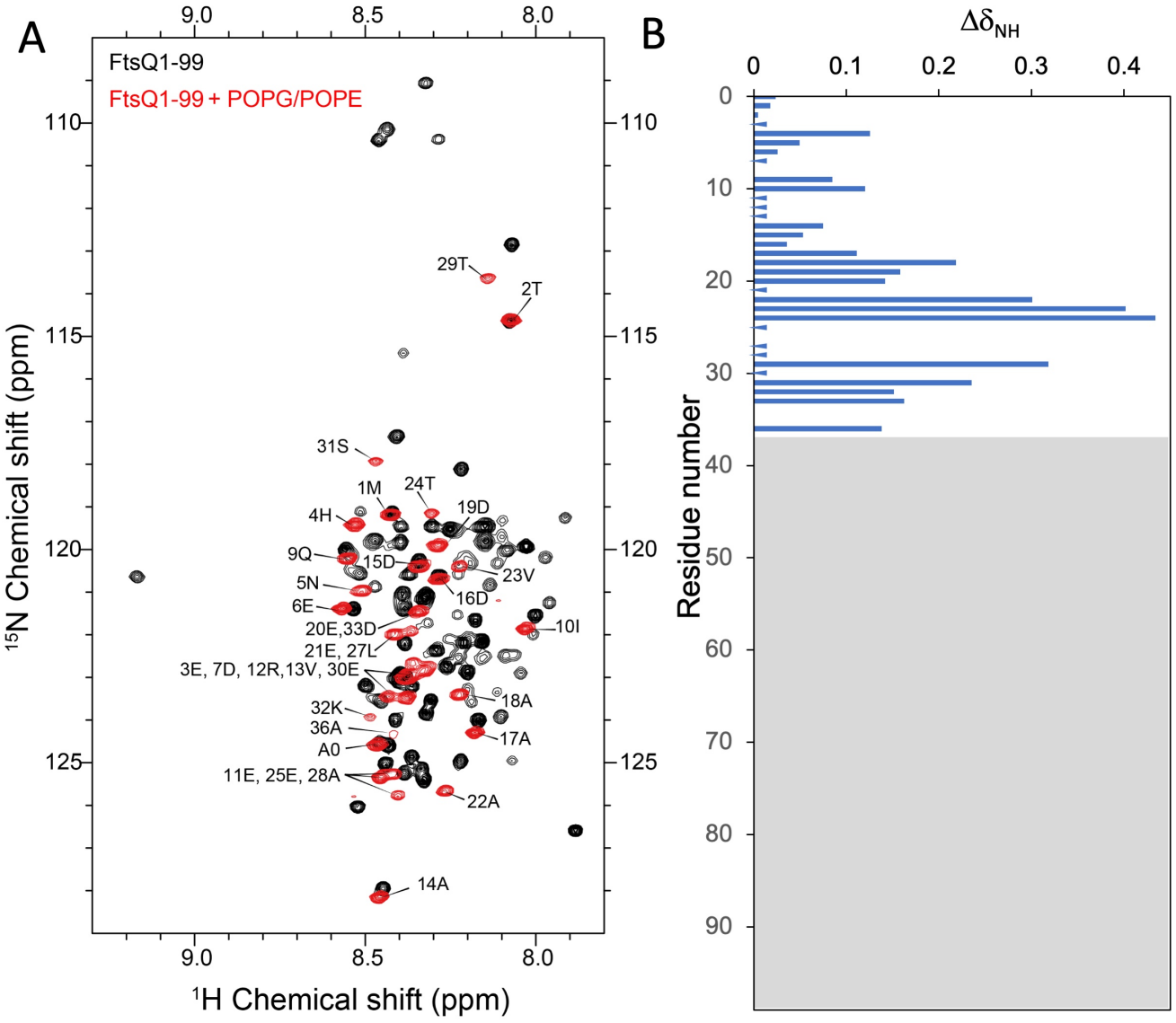
A
FtsQ1-99
FtsQ1-99 + POPG/POPE
9.0
8.5
8.0
110
115
120
125
^{15}N Chemical shift (ppm)
^{1}H Chemical shift (ppm)
29T
2T
31S
1M
24T
19D
4H
9Q
15D
23V
5N
16D
6E
20E,33D
10I
21E, 27L
3E, 7D, 12R,13V, 30E
18A
32K
36A
17A
A0
11E, 25E, 28A
22A
14A
B
$\Delta\delta_{NH}$
0
0.1
0.2
0.3
0.4
Residue number
0
10
20
30
40
50
60
70
80
90

Figure 2

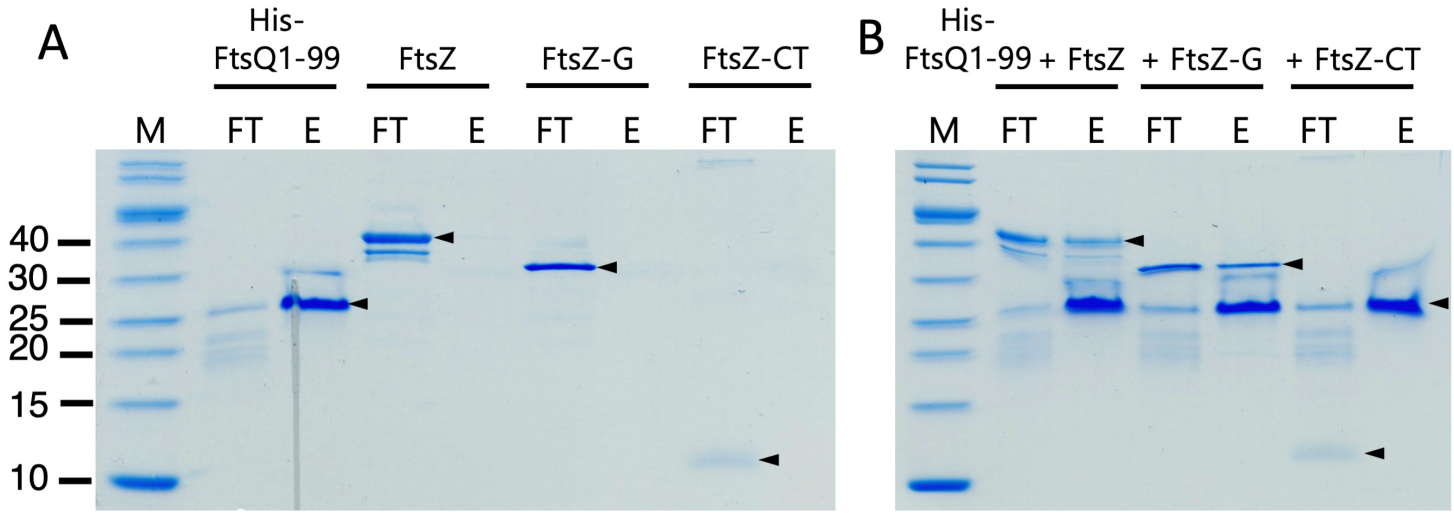
A
His-
FtsQ1-99
FtsZ
FtsZ-G
FtsZ-CT
M
FT
E
FT
E
FT
E
FT
E
40
30
25
20
15
10
B
His-
FtsQ1-99 + FtsZ
+ FtsZ-G
+ FtsZ-CT
M
FT
E
FT
E
FT
E

Figure 3

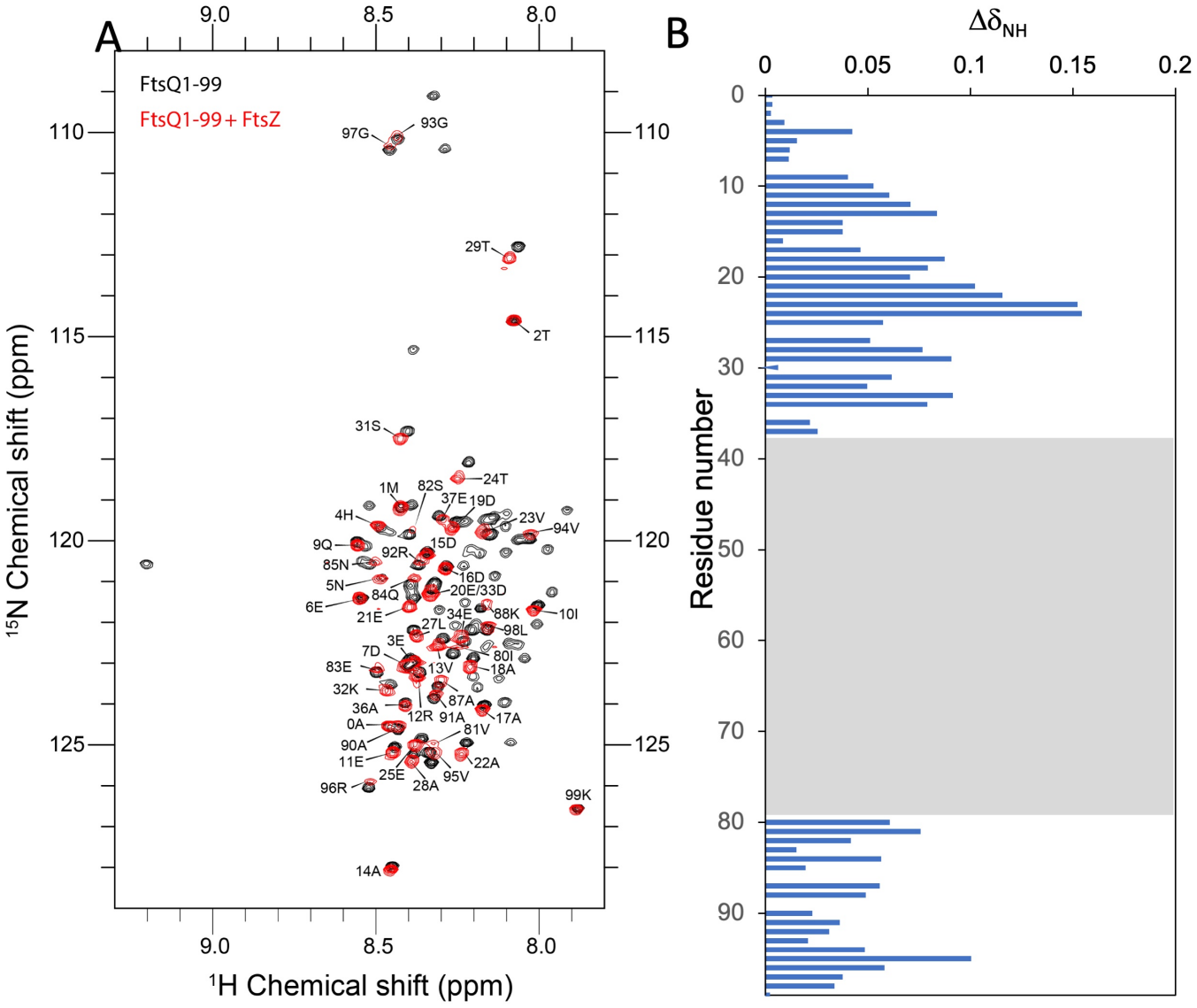
A
FtsQ1-99
FtsQ1-99 + FtsZ
97G
93G
29T
2T
31S
24T
1M
82S
37E
19D
4H
23V
94V
9Q
92R
15D
85N
16D
5N
84Q
20E/33D
6E
21E
34E
88K
10I
27L
98L
3E
7D
80I
83E
13V
18A
32K
87A
36A
12R
91A
17A
0A
81V
90A
22A
11E
25E
95V
96R
28A
99K
14A
^{15}N Chemical shift (ppm)
^{1}H Chemical shift (ppm)
B
$\Delta\delta_{NH}$
Residue number

Figure 4